Available online at www.sciencedirect.com

jmr&t Journal of Materials Research and Technology

www.jmrt.com.br

Original Article

Effect of nitrogen-doping on the surface chemistry and corrosion stability of TiO_2 films

*Edvan Almeida de Souza Filho, Eurico Felix Pieretti, Rodrigo Teixeira Bento, Marina Fuser Pillis**

Materials Science and Technology Center, Nuclear and Energy Research Institute (CCTM-IPEN/CNEN), São Paulo, Brazil

ARTICLE INFO

Article history:
Received 2 July 2019
Accepted 13 November 2019
Available online 29 November 2019

Keywords:
N-doped TiO_2films
TiO_2
MOCVD
Corrosion resistance

ABSTRACT

TiO_2 and N-doped TiO_2 films were grown on AISI 316 stainless steel substrates and on Si (100) by metallorganic chemical vapor deposition (MOCVD) at 400 °C and 500 °C. X-ray photoelectron spectroscopy, scanning electron microscopy, and contact angle techniques were used to characterize de films. The corrosion behavior was assessed by monitoring the open circuit potential, electrochemical impedance spectroscopy and potentiodynamic polarization tests in 3.5 wt% NaCl solution at room temperature. The results show that 6.18 at% of nitrogen was introduced in the films grown at 400 °C and 8.23 at% at 500 °C, and that besides TiO_2, nitrogen phases were identified. All the films are hydrophilic and the contact angles varied from 48° to 72°. The films presented good homogeneity, low porosity and rounded grains in the range of 40–90 nm. The RMS roughness varied between 5.5 and 18.5 nm. Titanium dioxide films grown at 400 °C showed better corrosion resistance than those grown at 500 °C due to its compact morphology. Nitrogen-doping was not efficient to protect the substrate from corrosion.

1. Introduction

Titanium dioxide has attracted significant interest for many applications, especially due to its stability and high corrosion resistance [1,2], availability, and low cost of production. It presents high dielectric constant and electrical resistivity, high refractive index, and good optical transparency in a wide spectral range. It is extensively used as cosmetics, pigments, building materials, bactericidal surfaces, photocatalysis, biocompatible devices, and solar cells [3–6]. TiO_2 is a transition metal oxide and presents three commonly polymorphs: TiO_2 anatase (tetragonal), brookite (orthorhombic), and rutile (tetragonal) [2,7]. Anatase phase is more stable than rutile at 0 K, but the difference in the enthalpy energy between these two phases is small (~ 2–10 kJ/mol) [8]. The anatase structure is preferred over other polymorphs for solar cell applications, due to the higher electron mobility, lower dielectric constant and lower density. The high photo reactivity is due to the higher Fermi level, the oxygen adsorption capacity and the higher degree of hydroxylation in the anatase phase [9]. The growth temperature of TiO_2 films produced by the MOCVD technique directly affects the structure of these films, and this structure is closely related to their corrosion stability,

* *Corresponding author.*
E-mail: mfpillis@ipen.br (M.F. Pillis).
https://doi.org/10.1016/j.jmrt.2019.11.032

Table 1 – Chemical composition of the AISI 316 stainless steel (wt %).

Elements										
	Fe	Cr	Ni	Mo	Mn	S	Si	P	N	C
Content	Bal.	17.08	10.29	2.27	1.57	0.72	0.35	0.06	0.10	0.12

and corrosion resistance in chlorine containing medium [10]. Several papers in the literature report on the use of TiO_2 films in the corrosion protection of metallic substrates [10–13].

The good electrical, optical and mechanical properties, besides thermal stability presented for the coatings in the Ti-O-N system makes it interesting for several technological applications. Titanium oxynitride coatings have been used as absorber films, anti-reflective coatings, diffusion barriers in semiconductors and high hardness metallurgical coatings [14]. The use of N-doped TiO_2 coatings as antibacterial surface on stainless steel [15], and as electrode in dye-sensitized solar cells [16] have been reported. Asahi et al. [17] proposed a method to elaborate N-doped TiO_2 anatase films, replacing oxygen atoms by nitrogen atoms. The small difference between the ionic radii of oxygen and nitrogen species would facilitate the substitution of oxygen and would not cause great distortion in the TiO_2 lattice [18]. The functional properties of TiO_2 as the refraction index, electrical conductivity, as well as the mechanical properties are altered according to the nitrogen content incorporated in the structure [19].

When high contents of nitrogen are incorporated into the TiO_2 film, titanium oxynitride TiO_xN_y may form, and the modification of the initial structure of the oxide occurs. On the other hand, for low nitrogen contents, the TiO_2 structure is maintained [20]. The structure of the TiO_xN_y film may be of the amorphous type, since the nitrogen is known to be a crystallization inhibitor, or cubic when there is a ternary solid solution between TiN and TiO with FCC phase. Results obtained by Duminica et al. [21] in the production of titanium oxynitride films grown by the MOCVD process show that ranging the nitrogen content in the films significant changes in the morphological, structural and mechanical characteristics occur. When a large excess of the nitrogen precursor is used, the film contains about 17 % nitrogen, and forms TiO_xN_y with a dense and amorphous structure. Wang et al. [15] studied the corrosion resistance in Hanks' solution of N-doped TiO_2 films deposited on AISI 304 stainless steel by plasma alloying technique. The results showed that the film was effective to protect the substrate, because the coating retards the local pitting and crevice corrosion of the stainless steel.

Several techniques are available for the synthesis of nitrogen-doped TiO_2 films, such as pulsed laser deposition [22], sputtering [23], sol gel [24], and CVD [18,20,21]. The CVD (chemical vapor deposition) technique consists of reacting compounds in the vapor phase, that are deposited on the surface of a heated substrate, forming a continuous and adherent film [25]. The metallorganic chemical vapor deposition (MOCVD) is a CVD process that uses organometallic compounds as precursors. This is an attractive process, since it needs lower temperatures of growth than the conventional CVD [25], presents high growth rates, besides allowing the covering of substrates with complex geometries. In this process the composition and structure of the films are determined by the chemical precursors used and by the deposition parameters [18,26,27]. This technique provides a good control of stoichiometry and thickness, uniformity of deposition and the possibility of covering large areas [28].

Table 2 – MOCVD process parameters.

Parameters	
Nitrogen purge gas flow rate (L/min)	0.5
Nitrogen carrier gas flow rate (L/min)	0.5
Ammonia flow rate (mL/min)	0.5
TTiP temperature (°C)	39
Substrate temperature (°C)	400 and 500
Growth pressure (mbar)	50

The aim of this work was to investigate the effect of nitrogen doping on the structure, morphology and electrochemical behavior of TiO_2 films grown by metallorganic chemical vapour deposition at the temperatures of 400 and 500 °C. The films were grown on AISI 316 substrates. For the characterisation atomic force microscopy, X-ray photoelectron spectroscopy (XPS), and field emission scanning electron microscopy (FE-SEM) analyses were done, besides electrochemical tests.

2. Material and methods

2.1. Substrates

Samples of AISI 316 stainless steel of 20 × 20 × 5 mm, and chemical composition (wt. %) presented in Table 1, were used as substrate. The samples were grounded in SiC papers, diamond polished until 3 μm, degreased in acetone, subsequently in ethanol, rinsed in deionized water, and dried in nitrogen prior of being inserted into the MOCVD reactor. Silicon wafers substrates were also used for convenience in order to determine the growth rate of the films. The surface preparation consisted in the immersion of the samples in a 5 %v H_2SO_4 water solution for 3 min, followed by rinsing in deionized water and drying in nitrogen.

2.2. Growth of the films

The 300 nm-thick films were produced in a conventional homemade MOCVD apparatus at the temperatures of 400 °C and 500 °C. For the production of TiO_2 films, only TTiP was used as titanium and oxygen sources, and to obtain N-doped TiO_2, ammonia (NH_3) was added to the system. Nitrogen was used both as the carrier gas to transport the TTiP into the system, and as purge gas. The process parameters are given in Table 2.

2.3. Characterisation

2.3.1. Scanning electron microscopy (SEM)

The cross section of the films grown on silicon substrates was evaluated by FE-SEM in a FEI Quanta 600 electronic microscope. The pits morphology on the surface after electrochemical tests was evaluated in a Hitachi table top microscope model TM3000.

2.3.2. Wettability tests

The surface hydrophilicity of films was evaluated by contact angle measurements in a SEO Phoenix-I equipment. The substrate and the films were stored for 120 h in a dark chamber before the tests to avoid the light interference. The sessile drop method was used by dropping 5 μL of deionized water on the surface. The experiments were done in triplicate for each sample.

2.3.3. Atomic force microscopy (AFM)

Surface topography, roughness measurements and mean grain size of the films were determined by atomic force microscopy operating in air in the tapping mode in a SPM Bruker NanoScope IIIA equipment with a silicon tip under ambient conditions. The AFM images were carried out on 2 μm × 2 μm surface area.

2.3.4. X-ray photoelectron spectroscopy (XPS)

X-ray photoelectron spectroscopy (XPS) analyses were carried out to determine the chemical state of the species close to the solid surface. A Thermo Scientific, K-Alpha model equipment and a spot beam of 400 μm was provided. The high-resolution spectra of Ti2P, O1s and N1s were acquired, and the deconvolution was performed using the algorithm Smart in the software Avantage®. The binding energies were corrected based on the C1s reference peak at 284.8 eV.

2.3.5. Electrochemical behaviour

The electrochemical tests were carried out using a potentiostat-galvanostat EG&G - Princeton Applied Research, Model 273A, with a flat-cell of three electrodes composed of a working electrode with 1.0 cm^2 of exposed area, a counter-electrode of platinized platinum and a Saturated Calomel Electrode (SCE) (3 M) as reference. The tests were conducted at room temperature in a 3.5 wt. % NaCl, and the applied potential varied from −600 mV to 2500 mV. The scanning rate was 1.0 mV/s. Before the potentiodynamic polarization tests the surfaces were evaluated by monitoring the open circuit potential *vs.* time and electrochemical impedance spectroscopy.

3. Results and discussion

3.1. FE-SEM characterization

Fig. 1 shows the cross-section of TiO_2 and N-TiO_2 films grown at 400 °C and 500 °C on Si (100). It can be observed that the interface between the film and the substrate is flat, and that the films grow perpendicular to the surface of the substrate. In the figure it is also possible to observe significant morphological differences between the films. While films grown at 400 °C independently of the doping present a densified morphology, films grown at 500 °C show columnar morphology suggesting that these films present a high level of porosity. The growth rate was estimated by dividing the film thickness by the time of growth. The values found were of 13 and 8 $nm.min^{-1}$ for undoped and doped TiO_2 grown at 400 °C, respectively, and of 37 and 10 $nm.min^{-1}$ for TiO_2 and N-TiO_2 grown at 500 °C, respectively. Based on these results 300 nm-thick films were grown on AISI 316 SS substrates.

3.2. Wettability tests

Fig. 2 exhibits the contact angle measurements of the undoped and N-doped TiO_2 films, as well as for the AISI 316 substrate. It was found that the contact angle for water was 77° for the steel substrate (Fig. 2a). Undoped TiO_2 film grown at 400 °C (Fig. 2b) presented a contact angle value around 68°, while the measurement for the undoped film grown at 500 °C (Fig. 2c) was of 72°. For the doped films the contact angle measurements decreased for 61° and 48°, respectively, for the N-doped films at 400 °C (Fig. 2d) and 500 °C (Fig. 2e).

The results showed that all the films are hydrophilic and suggested that the N-doping process improves the hydrophilicity of TiO_2 films together with the growth temperature, as it is indicated in Table 3. Surfaces that present contact angles $\leq 90°$ are referred as hydrophilic ones whereas contact angles greater than 90° corresponds to hydrophobic surfaces [29–31]. The main factors that influence the wettability of surfaces are the superficial microstructure and the chemical composition [32,33].

3.3. AFM characterisation

Figs. 3 and 4 show the surface topography and the three-dimensional AFM images of the TiO_2 films grown at 400 °C and 500 °C, respectively. Figs. 5 and 6 show the surface of the N-TiO_2 films grown at 400 °C and 500 °C, respectively. The films presented good homogeneity, low porosity and rounded grains in the range of 40–90 nm. The images show that TiO_2 grains have grown following the marks left in the substrate by the polishing step. The insert in Figs. 3–6b reveals the columnar structure of the films, that grows perpendicularly to the substrate, as it was described in the literature [18,34], and shown previously by the SEM images. The increase in the growth temperature, promoted the increase of the roughness values and the mean grain size of the films, as it can be seen in Table 3, which suggests an increase on its crystallinity.

The nitrogen doping provoked a decrease in both the RMS roughness and grain size for the undoped and doped TiO_2 films grown at 400 °C and 500 °C. Oja Acik et al. [35] suggested that the doping process stimulate the growth of individually grains. Rojviroon et al. [36] obtained similar trend. The authors deposited TiO_2 and Fe-doped TiO_2 films on 304 stainless steel substrates. The TiO_2 films showed a surface roughness of 18.3 nm, while the 0.3 % Fe-TiO_2 and 0.7 % Fe-TiO_2 films exhibited 11.92 nm and 12.92 nm, respectively. Duminica et al. [21] have grown N-doped TiO_2 films on stainless steel by MOCVD. The films grown at 400 °C presented roughness values around 10 nm – close to the values obtained in the present study. The

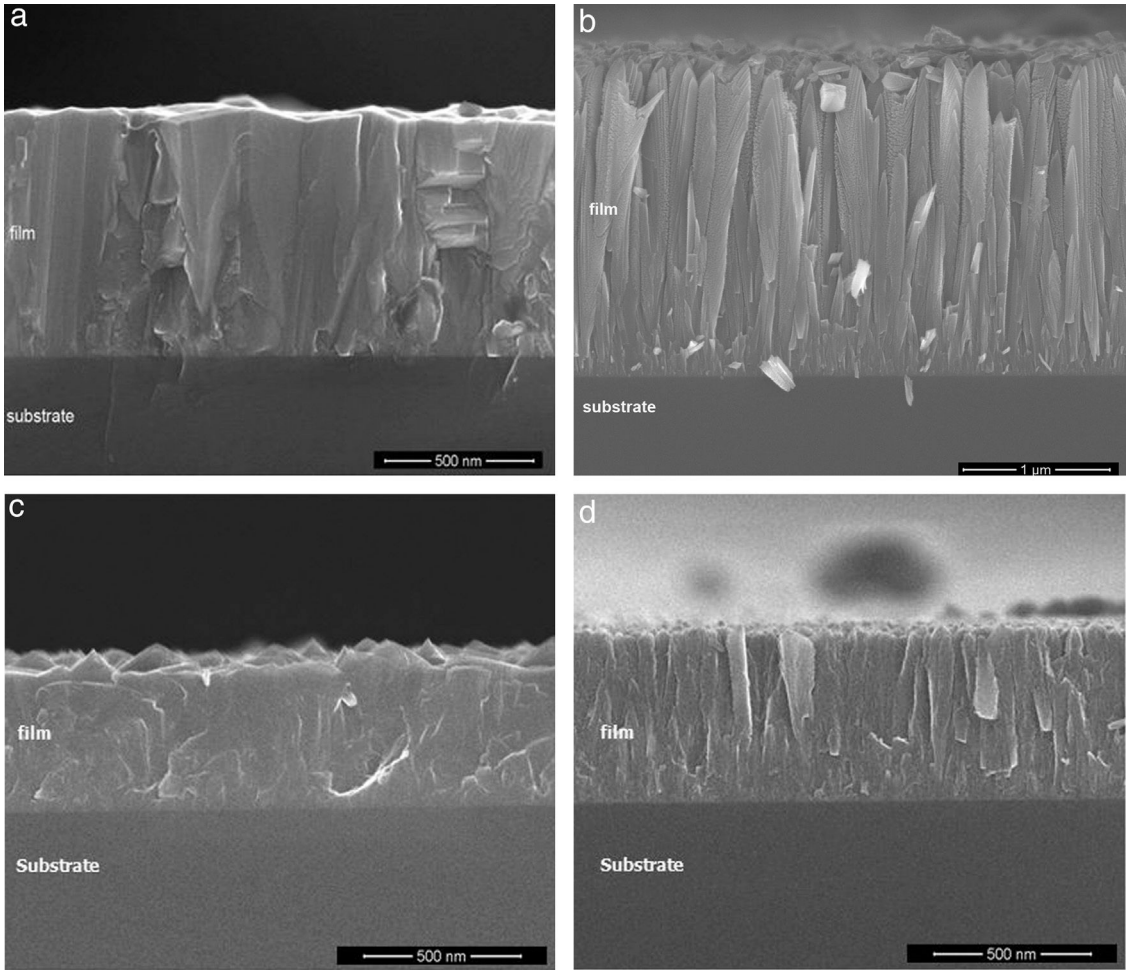

Fig. 1 – Scanning electron microscopy images of the cross section of films grown for 60 min on Si (100). (a) TiO_2 grown at 400 °C; (b) TiO_2 grown at 500 °C; (c) N-doped TiO_2 at 400 °C and (d) N-doped TiO_2 grown at 500 °C.

Table 3 – Surface parameters of uncoated and coated stainless steel.

Sample	Deposition temperature [°C]	RMS roughness [nm]	Mean grain size [nm]	Mean contact angle [°]
Substrate	–	9.6	–	77
TiO_2 film	400	12.2	75.8	68
TiO_2 film	500	18.5	87.7	72
N-TiO_2 film	400	5.5	43.6	61
N-TiO_2 film	500	14.7	59.7	48

authors suggested that the presence of nitrogen at this temperature leads to the amorphization of the films.

3.4. *XPS characterisation*

The XPS technique was used to analyse the composition and binding energies between the atoms that compose the N-doped TiO_2 films obtained at 400 °C and 500 °C. Fig. 7 shows the XPS survey spectrum of the N-doped TiO_2 films grown at both temperatures. The peak near 400 eV shows that nitrogen was successfully incorporated into the films. The main components were quantified and the results are listed in Table 4. It is well known that the exposition of the sample to the air results in the contamination by carbon [37]. In addition, residual carbon due to the decomposition of the metallorganic precursor may also be incorporated into the film [37,38]. The carbon content decreases as the growth temperature increases [37].

Fig. 8a–f show the high-resolution XPS core-level spectra of the nitrogen-doped films grown at 400 °C and 500 °C. The chemical bonding states obtained by deconvoluting and fitting the curves are presented in Table 5. Fig. 8a and b show these spectra in the Ti 2p energy region. The doublets of Ti2p at 459.1 eV ($2p_{3/2}$) and 464.8 eV ($2p_{1/2}$) for the films grown at 400 °C and at 458.8 eV ($2p_{3/2}$) and 464.5 eV ($2p_{1/2}$) for the films grown at 500 °C are associated with anatase TiO_2. Thus, the highest contribution is due to Ti^{+4}, which corresponds to the contributions of Ti^{+4} $2p_{1/2}$ and $2p_{3/2}$ of TiO_2. These results are in good agreement to the literature [20,21,37,39,40]. The lower energy titanium peak values suggest the formation of Ti-N bonds, and when accompanied by a Ti 2p peak enlargement, confirms the

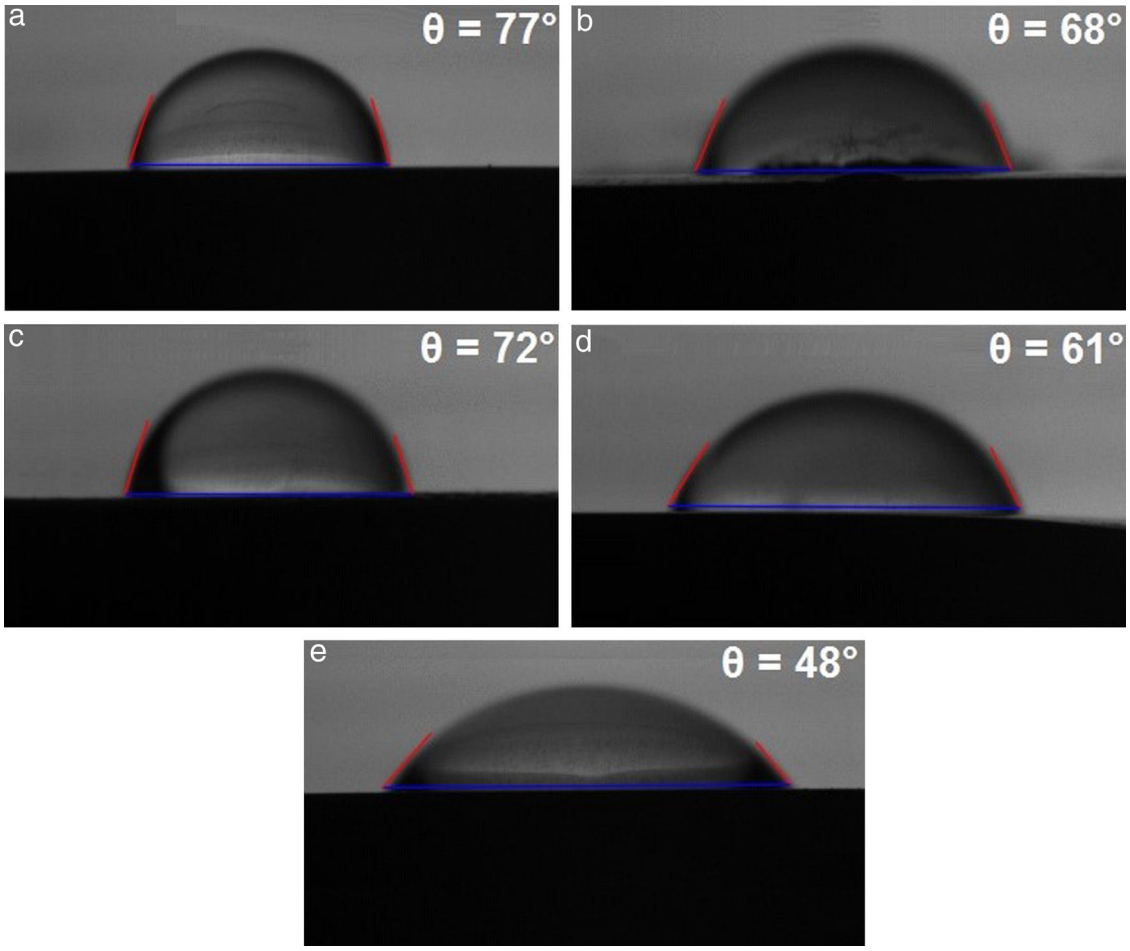

Fig. 2 – Contact angle measurements. (a) uncoated 316 and coated (b) TiO_2 film grown at 400 °C; (c) TiO_2 film grown at 500 °C; (d) N-doped TiO_2 film grown at 400 °C; (e) N-doped TiO_2 film grown at 500 °C.

Table 4 – Atomic concentration of Ti2p, O1s, N1s and C1s elements.

Growth temperature (°C)	Ti2p (at.%)	O1s (at.%)	N1s (at.%)	C1s (at.%)
400	26.70	48.79	6.18	18.33
500	26.53	52.37	8.23	12.87

Table 5 – The binding energies (BE) of the bonds of N-doped films grown at 400° and 500 °C.

	400 °C			500 °C		
Component	BE (eV)	FWHM	at.%	BE (eV)	FWHM	at.%
Ti^{4+} $2p_{3/2}$	459.1	1.45	47.35	458.8	1.63	50.81
Ti^{4+} $2p_{1/2}$	464.8	2.32	26.58	464.5	2.47	27.45
Ti^{3+} $2p_{3/2}$	457.8	2.34	9.03	457.2	1.89	6.17
Ti^{3+} $2p_{1/2}$	461.2	4.71	17.04	461.2	4.42	15.57
N1s	396.7	1.06	77.97	396.6	1.05	71.21
	397.3	1.70	12.65	397.1	1.89	22.55
	401.1	3.37	9.38	401.7	2.69	6.25
O1s	530.8	1.30	74.42	530.6	1.33	64.57
	531.6	2.57	25.58	531.7	2.39	35.43

contribution of Ti^{+3}, originating from nitride or oxynitride [21]. The peaks found at 457.89 eV and at 463 eV are due to N-Ti-N and/or O-Ti-N bonds [21,41].

Fig. 8c and d show the high-resolution XPS core-level spectra of the nitrogen-doped films grown at 400 °C and 500 °C in the N1s energy region. Table 5 shows the chemi-

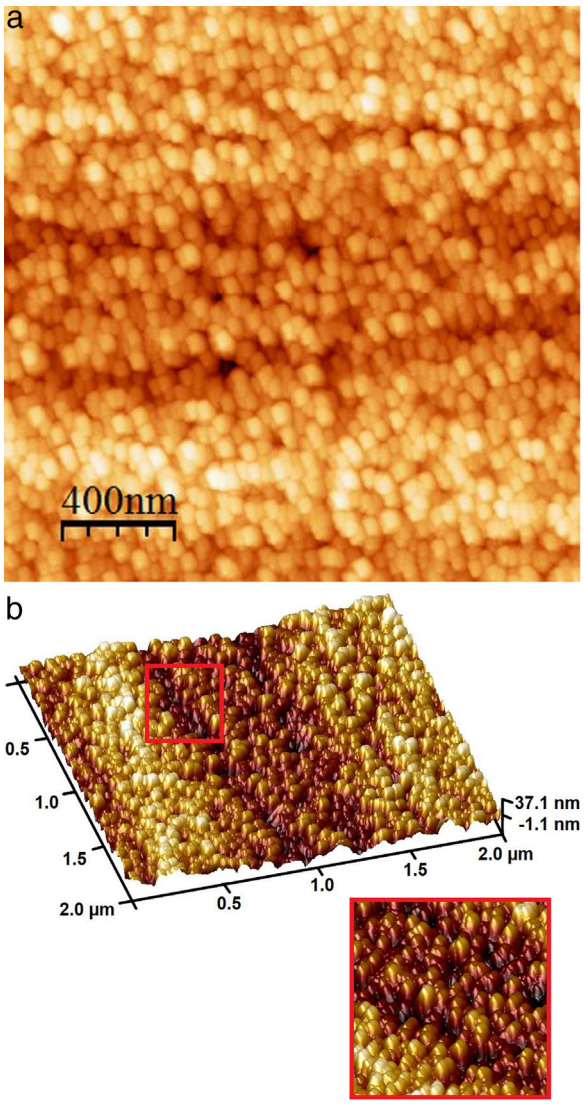

Fig. 3 – AFM surface images of the TiO_2 film grown at 400 °C. (a) topography; (b) 3D image. The insert shows the typical columnar structure of the film in details.

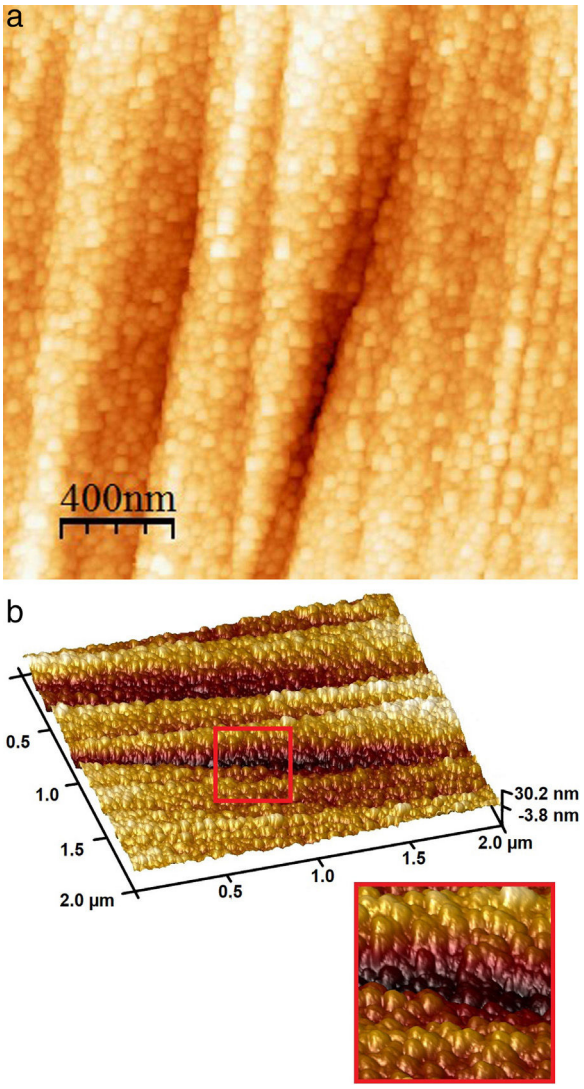

Fig. 4 – AFM surface images of the TiO_2 film grown at 500 °C. (a) topography; (b) 3D image. The insert shows the typical columnar structure of the film in details.

cal bonding states obtained by deconvoluting and fitting the curves. The peaks at 396.7 eV and 396.6 eV for films grown at 400 °C and 500 °C, respectively, can be attributed to substitutional nitrogen (β-N) replacing oxygen in the lattice in TiN_xO_y [17,20,39,42]. The peaks centered at 397.3 eV and 397.1 eV for films grown at 400 °C and 500 °C can be attributed to Ti-N [42,43]. A broad peak centered on 401 eV was found in the spectra. According to Chen and Burda [44], a broadening peak centered at 401.3 eV can be attributed to O-Ti-N bonds.

Fig. 8e and f show the high-resolution XPS core-level spectra of the nitrogen-doped films grown at 400 °C and 500 °C in the O1s energy region. The peaks at 530.8 eV and 530.6 eV for the films grown at 400 °C and 500 °C, respectively are related to Ti-O linkages in TiO_2 [21,38,39,42]. The peaks at around 531.6 eV are attributed to adsorbed water, corresponding to oxygen in hydroxyl groups [21,42].

3.5. *Electrochemical behavior*

The corrosion resistance of the AISI 316 stainless steel samples was evaluated by electrochemical methods analyzing an area corresponding to 1 cm^2. The results show the reproducible behavior obtained in 3 trials for each condition.

The open circuits potential vs. immersion time (OCP) curves for uncoated and 300 nm-thick coated AISI 316 stainless steel are presented in Fig. 9. The sample covered by N-doped TiO_2 film grown at 400 °C showed a slight increase in its potential in the initial minutes of the test and then a constant decrease of the potential as the immersion time increases. The sample covered by the N-doped TiO_2 film grown at 500 °C showed a sudden drop in the first minutes, and soon after, a tendency to stabilization. For the undoped film grown at 400 °C the curve suggests the breakdown and recomposition of the passive layer in the first half of the test but shows a tendency to stabilize at a potential close to the substrate.

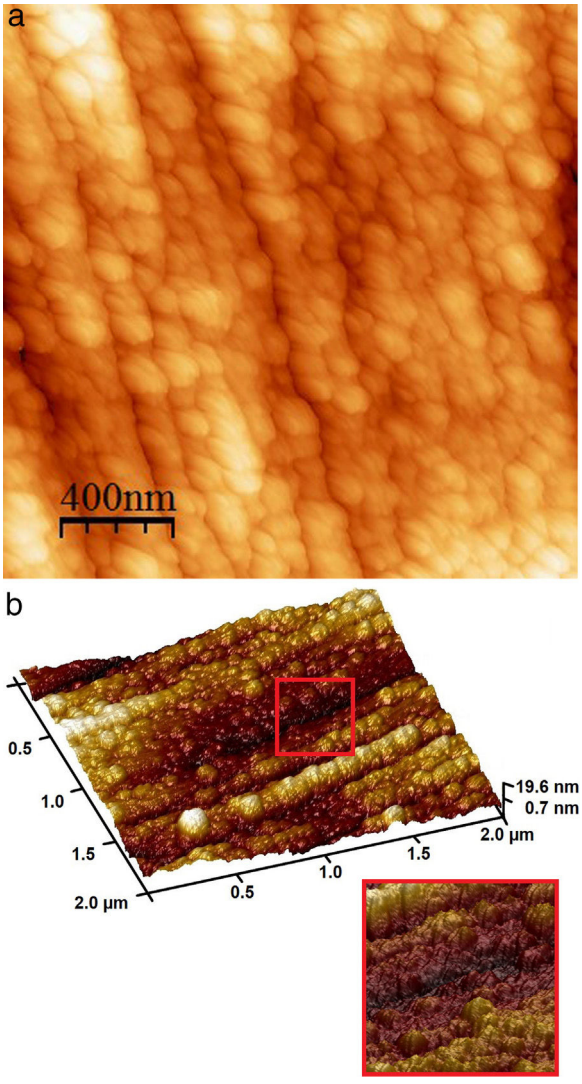

Fig. 5 – AFM surface images of the N-doped TiO_2 film grown at 400 °C. (a) topography; (b) 3D image. The insert shows the typical columnar structure of the film in details.

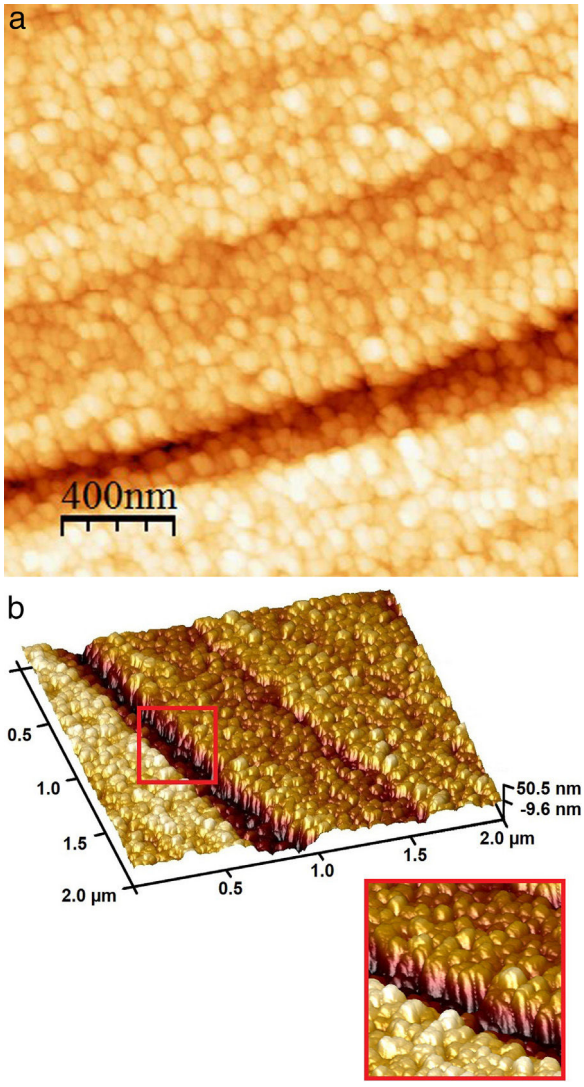

Fig. 6 – AFM surface images of the N-doped-TiO_2 film grown at 500 °C. (a) topography; (b) 3D image. The insert shows the typical columnar structure of the film in details.

The sample coated with TiO_2 film grown at 500 °C presented a more homogeneous behavior in the same immersion periods in 3.5 % p NaCl, in relation to its pairs, and shows greater stability of the film. Nitrogen doped films showed stabilization in OCP lower than those presented by the samples covered by undoped films. In addition, films grown at 400 °C stabilize at higher potentials than those grown at 500 °C.

The anti-corrosion properties of these coatings were evaluated via electrochemical impedance spectroscopy (EIS). For comparison reasons the substrate without coatings was also evaluated and the results are presented in Fig. 10. The tests were performed after OCP and prior to polarization, and all coatings showed inferior impedance values comparing to the substrate. Nyquist plots revealed that the films grown at 400 °C presented higher impedance than films grown at 500 °C for both conditions and N- doped TiO_2 film grown at 500 °C presented the minor value, corresponding to a lesser protective behavior.

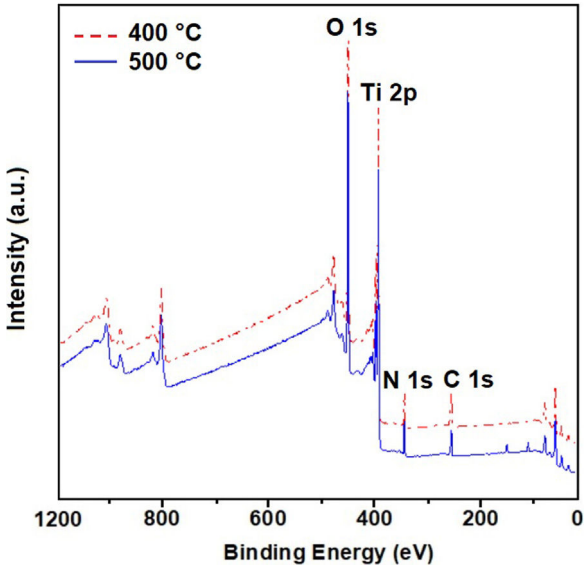

Fig. 7 – XPS survey spectra of N-doped TiO_2 films grown at 400 and 500 °C.

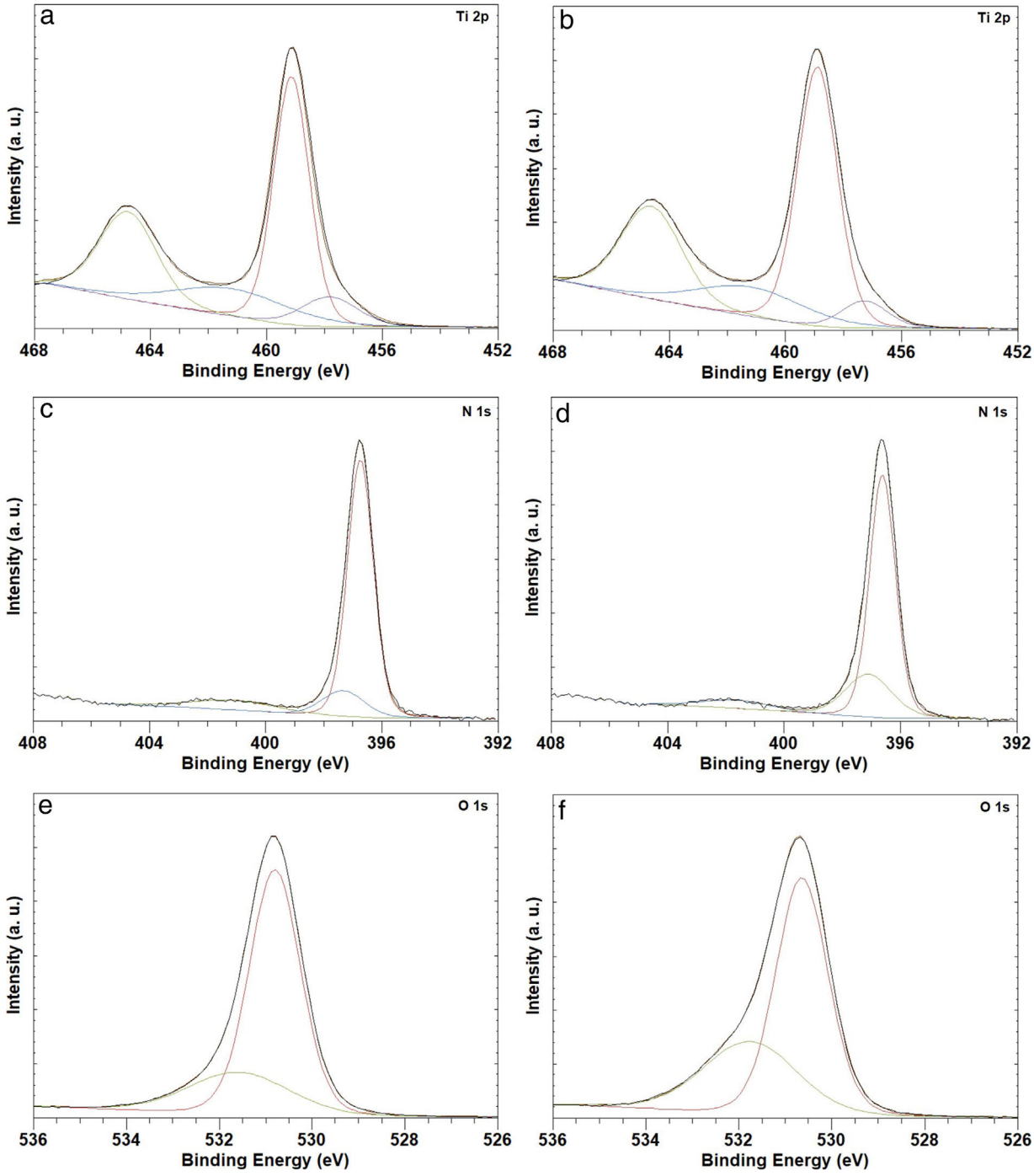

Fig. 8 – XPS core-level spectra of the N-doped TiO_2 films grown at 400 °C (a, c, e) and at 500 °C (b, d, f).

Table 6 – EIS fitting parameters adjusted using the ECs shown in Fig. 11 for uncoated and titanium-based coated AISI 316 austenitic stainless steel.

	R1 ($\Omega.cm^2$)	CPE2 ($cm^{-2}s^{-n}\Omega$)	n 2	R2 ($\Omega.cm^2$)	C3 ($cm^{-2}s^{-n}\Omega$)	R3 ($\Omega.cm^2$)
Substrate	376.9	2.12×10^{-5}	0.8579	1.20×10^{6}	–	–
TiO_2 400º	377.7	2.02×10^{-5}	0.8661	1.67×10^{5}	1.76×10^{-6}	9.28×10^{5}
TiO_2 500º	287.0	9.40×10^{-6}	0.9154	1.49×10^{6}	7.74×10^{-6}	8.68×10^{5}
N-TiO_2 400º	377.5	1.89×10^{-5}	0.7259	983.8	1.82×10^{-5}	1.23×10^{6}
N-TiO_2 500º	201.9	1.80×10^{-4}	0.4534	498.8	5.95×10^{-5}	4.23×10^{5}

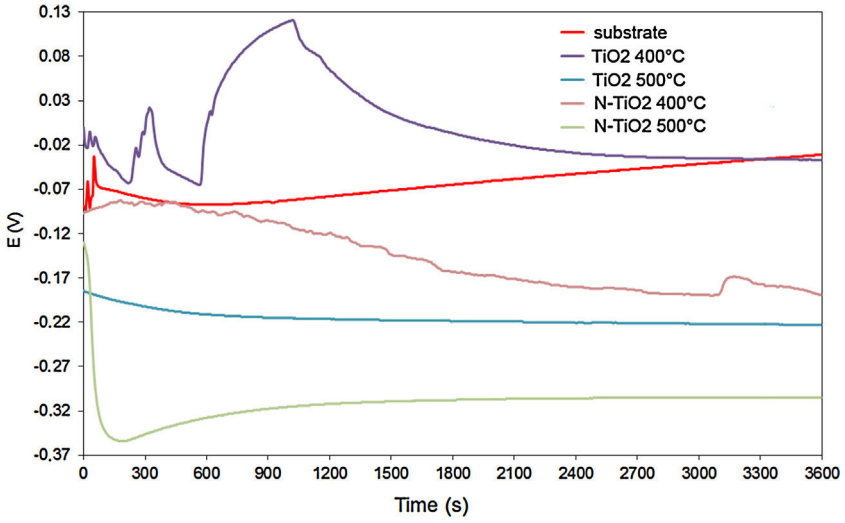

Fig. 9 – Open circuit potential curves for the substrate, TiO_2 and N-doped TiO_2 films.

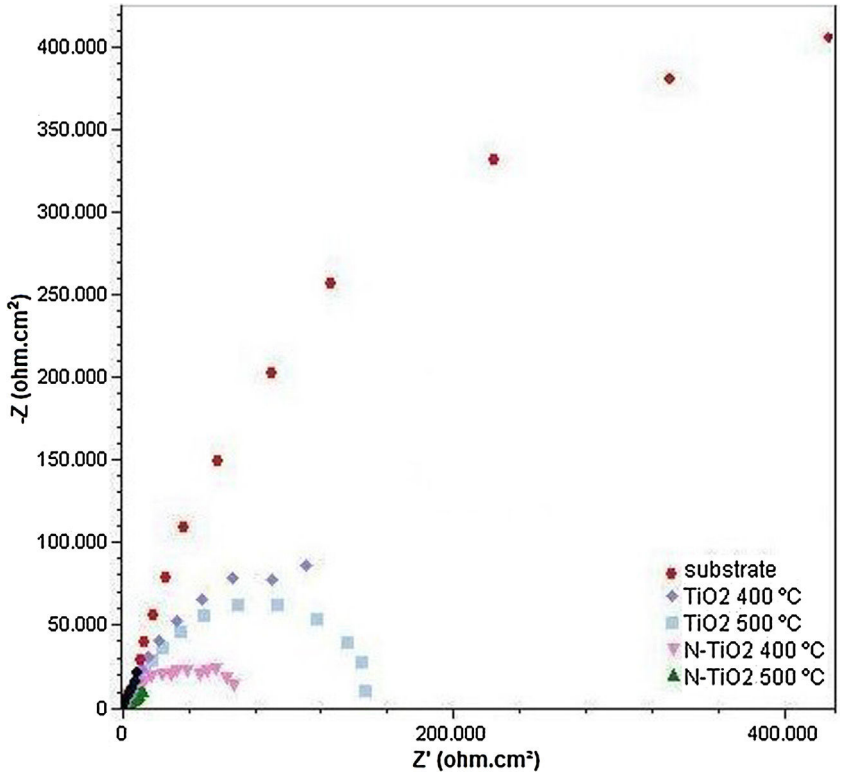

Fig. 10 – Electrochemical impedance spectroscopy (Nyquist plots) for the substrate, TiO_2 and N-doped TiO_2 films grown at 400 °C and 500 °C.

Fig. 11 shows two separate electrical equivalent circuits (EEC) that were used to model the EIS data. This approach is commonly present in the literature [45–47]. The CPE is the constant phase element, C is the capacitance, R1 is the solution resistance, R2 is the titanium oxide based-film resistance and R3 is the passive layer resistance. The circuit shown in Fig. 11a was the one that best fits the uncoated sample. In Fig. 11b it can be seen the EEC for the coated specimens. The extracted values are presented in Table 6.

The lowest n2 values were found for N-TiO_2 samples. The capacitance CPE2 is associated to the resistance R2. The values presented for N-TiO_2 sample at 500 °C are one order of magnitude higher than those obtained for the uncoated (substrate) sample. This result indicates the presence of a more defective film on this surface. The inner layer resistance R3, which is related to chromium oxides, showed values for N-TiO_2 samples five and six orders of magnitude higher for the films grown

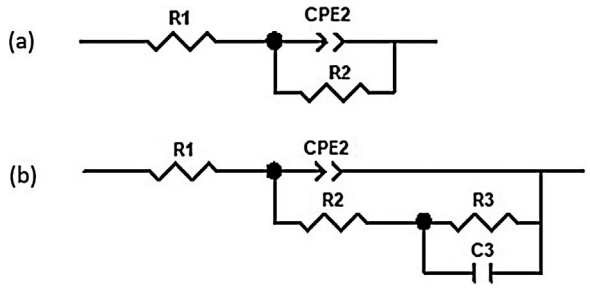

Fig. 11 – ECs used to simulate the EIS experimental data: (a) uncoated AISI 316 stainless steel; (b) coated AISI 316 stainless steel.

at 500 and 400 °C, respectively, than those obtained for the same films for R2.

Fig. 12 shows the linear polarization curves for the substrate, TiO_2 and N-doped TiO_2 films grown at 400 °C and 500 °C. It can be observed that the substrate presents well-defined passive layer formation with corrosion potential of −276 mV and corrosion current of 0.163 μA.cm^{-2}. The breakdown of the passive film occurred at approximately +440 mV. The TiO_2 covered at 400 °C sample presents values of corrosion potential a little nobler than the substrate, and corrosion current density about an order of magnitude lower. It presents a passive region with breaking potential of 482 mV, very close to the uncoated steel. The sample covered by the N-doped TiO_2 film grown at 400 °C showed potential and corrosion current similar to the undoped film and presents a very discrete passive region. The samples coated at 500 °C with TiO_2 and N-doped TiO_2 films showed no passive film formation, and the curves are representative of film dissolution. It is observed that the films produced at 500 °C showed a tendency to dissolve, apart they were doped or not.

Values of corrosion potential (E_{corr}), break potential (E_{break}), and corrosion current density (i_{corr}) were determined from the polarization curves and are displayed in Table 7.

Table 7 – Electrochemical parameters determined from the potentiodynamic polarization curves shown in Fig. 12.

	E_{corr} (mV_{SCE})	E_{break} (mV_{SCE})	I_{corr} (μA. cm^{-2})
Uncoated	−276	+440	0.163
TiO_2 400 °C	−32	+482	0.342
TiO_2 500 °C	−220	–	0.293
N-TiO_2 400 °C	−182	78	0.117
N-TiO_2 500 °C	−318	–	0.764

The shift on the corrosion potential for TiO_2 and N-doped TiO_2 samples obtained at 400 °C may be explained by the morphology obtained that diminish the access of the NaCl solution to the substrate. Similar results were found for AISI 316 L SS and AISI 304 L SS coated by titanium oxides in different media [48–50].

Fig. 13a and b show the surface of the sample covered by TiO_2 at 400 °C after potentiodynamic polarization test, evidencing corrosion pits on the film that exposes the substrate. The substrate dissolution under the TiO_2 layer is evidenced in this figure, which corroborates the passive behavior presented by this sample. However, despite the passivation, the passive film breaking potential was in the same order that the substrate. Fig. 14 shows the surface of the stainless steel AISI 316 covered by an N-doped TiO_2 film of grown at 400 °C, after potentiodynamic polarization test in 3.5 % NaCl solution at room temperature and shows the delamination of the film.

TiO_2 films grown at 400 °C tend to offer better alloy protection than those grown at 500 °C, probably due to the microstructural characteristics. Films grown at 500 °C showed a columnar structure, which represents a high level of porosity, while the films grown at 400 °C presented a denser structure. Similar results were reported by Antunes et al. [10]. In relation to the nitrogen-doping, the contents added not only do not protect the alloy, but also showed a deleterious effect on its corrosion resistance. A possible explanation is the formation of nitrogen-rich phases besides TiO_2. Furthermore, the surface of the samples is hydrophilic, that is, has high affinity

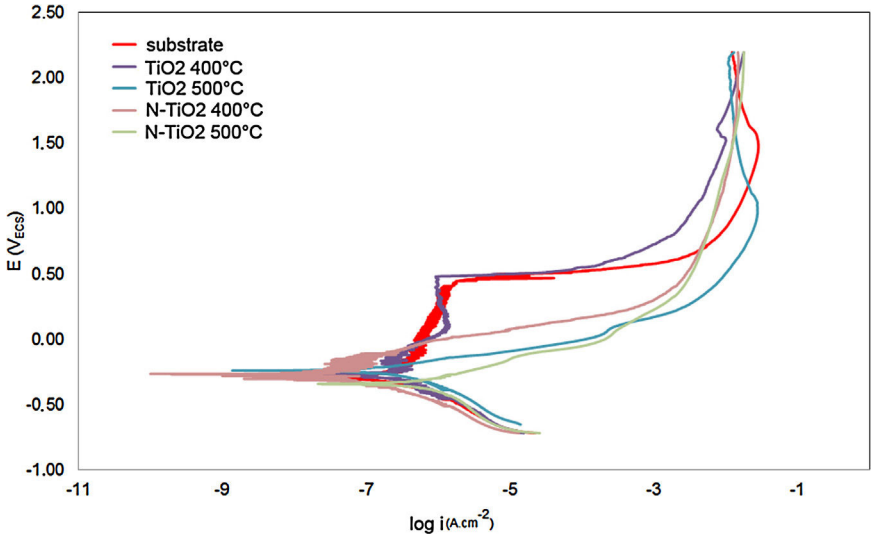

Fig. 12 – Linear polarization curves for the substrate, TiO_2 and N-doped TiO_2 films grown at 400 °C and 500 °C.

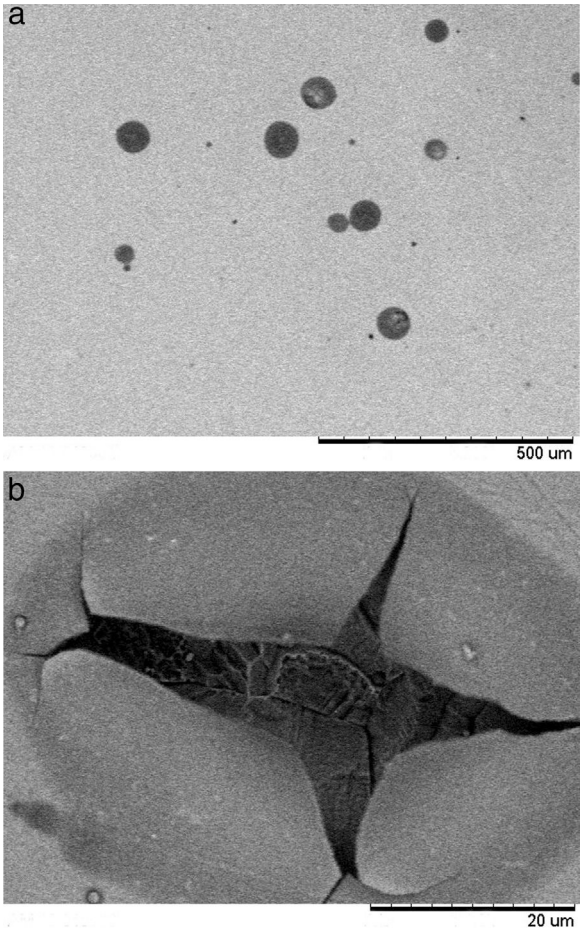

Fig. 13 – (a) Surface of stainless steel AISI 316 covered by a TiO_2 film grown at 400 °C, after potentiodynamic polarization test in 3.5 % NaCl solution at room temperature; (b) higher magnification in a region of (a).

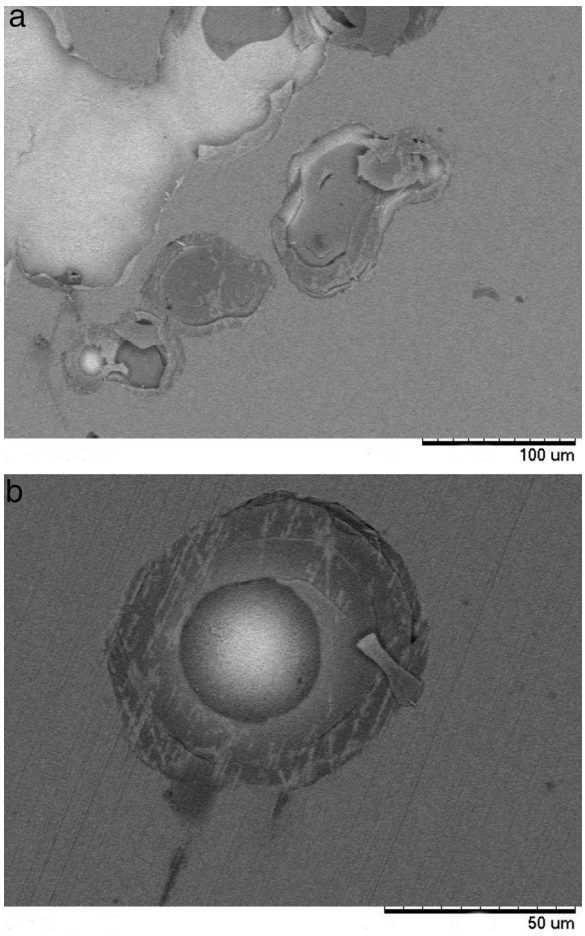

Fig. 14 – (a) Surface of the stainless steel AISI 316 covered by a of N-doped TiO_2 film grown at 400 °C, after potentiodynamic polarization test in 3.5 % NaCl solution at room temperature showing delamination of the film; (b) higher magnification in a region of (a).

for water [51] and affects the corrosion behavior of the films [52].

The corrosion process in the films starts at the films surface that is in contact with the aggressive medium. A pit is formed in the film, which allows the corrosive medium to access the metallic substrate. The metal is attacked and dissolved under the film, and results in its delamination.

4. Conclusions

Undoped and nitrogen-doped TiO_2 films were grown on AISI 316 stainless steel substrates by the metallorganic chemical vapour deposition technique using titanium tetraisoproxide as titanium and oxygen precursors, and ammonia as nitrogen source. It was shown that the growth temperature influences the films morphology, the phases formed, as well as the nitrogen content incorporated into the films. All the films showed columnar morphology; however, at 500 °C the microstructure is more porous.

Nitrogen was successfully incorporated into the TiO_2 films in a content of 6.18 at% at 400 °C and 8.23 at% at 500 °C. Besides TiO_2, nitrogen-rich phases were identified in the films. All the films presented hydrophilic characteristics and the contact angles varied from 48° to 72°.

The films presented good homogeneity, low porosity and rounded grains in the range of 40–90 nm. The increase in the growth temperature, promoted the increase of the roughness values and the mean grain size of the films.

TiO_2 films grown at 400 °C showed better corrosion protection than those grown at 500 °C, due to their microstructural differences. Films grown at 500 °C showed a porous columnar structure, which represents a high level of porosity that favours the access of the electrolyte, while the films grown at 400 °C presented a denser columnar structure. Nitrogen doping, in the incorporated contents, was not efficient to protect the substrate from corrosion possibly due to the formation of the nitrogen-rich phases.

Conflict of interest

The authors declare no conflict of interest.

Acknowledgements

The authors are thankful to the Brazilian Nanotechnology National Laboratory - LnNano for XPS analyses, and to the Brazilian agencies CAPES, CNPq (Proc. 168935/2018-0) and FAPESP (Proc. 05/55861-4) for the financial support.

REFERENCES

[1] Kim C, Choi C, Jang J. Nitrogen-doped SiO_2/TiO_2 core/shell nanoparticles as highly efficient visible light photocatalyst. CatalCommun 2010;11:378–82.
[2] Reddy KM, Manorama SV, Reddy AR. Bandgap studies on anatase titanium dioxide nanoparticles. Mater Chem Phys 2002;78:239–45.
[3] Nasu A, Otsubo Y. Rheology and UV-protecting properties of complex suspensions of titanium dioxides and zinc oxides. J Coll Interf Sci 2007;310:617–23.
[4] Evans P, Sheel DW. Photoactive and antibacterial TiO_2 thin films on stainless steel. Surf Coat Technol 2007;201:9319–24.
[5] Schmidt-Mendes L, Gratzel M. TiO_2 pore-filling and its effect on the efficiency of solid-state dye-sensitized solar cells. Thin Solid Films 2006;500:296–301.
[6] Bento RT, Correa OV, Pillis MF. Photocatalytic activity of undoped and sulfur-doped TiO_2 films grown by MOCVD for water treatment under visible light. J Eur Ceram Soc 2019;39:3498–504.
[7] Thamaphat K, Limsuwan P, Ngotawornchai B. Phase characterization of TiO_2 powder by XRD and TEM. Nature Sci 2008;42:357–61.
[8] Muscat J, Swamy V, Harrison NM. Principles calculations of the phase stability of TiO_2. Phys Rev B 2002;65:1–15.
[9] Tanaka K, Capule MF, Hisanaga T. Effect of crystallinity of TiO_2 on its photocatalytic action. Chem Phys Lett 1991;187:73–6.
[10] Antunes RA, Oliveira MCL, Pillis MF. Effect of the deposition temperature on the corrosion stability of TiO_2 films prepared by metal organic chemical vapor deposition. Int J Electrochem Sci 2013;8:1487–500.
[11] Popescu S, Demetrescu I, Sarantopoulos C, et al. The biocompatibility of titanium in a buffer solution: compared effects of a thin film of TiO_2 deposited by MOCVD and of collagen deposited from a gel. J Mater Sci Mater Med 2007;18:2075–83.
[12] Xie D, Wang H, Ganesan R, et al. Fatigue durability and corrosion resistance of TiO_2 films on CoCrMo alloy under cyclic deformation. Surf Coat Technol 2015;275:252–9.
[13] Chen S, Guan S, Chen B, et al. Corrosion behavior of TiO_2 films on Mg-Zn alloy in simulated body fluid. Appl Surf Sci 2011;257:4464–7.
[14] Lee DN. A model for development of orientation of vapor deposits. J Mater Sci 1989;24:4375–8.
[15] Wang H, Tang B, Li X, et al. Antibacterial properties and corrosion resistance of nitrogen-doped TiO_2 coatings on stainless steel. J Mater Sci Technol 2011;27:309–16.
[16] Guo W, Shen Y, Wu L, et al. Effect of N dopant amount on the performance of dye-sensitized solar-cell based on N-doped TiO_2 electrodes. J Phys Chem C 2011;115:21494–9.
[17] Asahi R, Morikawa T, Ohwaki T, et al. Visible-light photocatalysis in nitrogen-doped titanium oxides. Science 2001;293:269–71.
[18] Sarantopoulos C, Gleizes AN, Maury F. Chemical vapor deposition and characterization of nitrogen doped TiO_2 thin films on glass substrates. Thin Solid Film 2009;518:1299–303.
[19] Rocha LA, Ariza E, Ferreira J, et al. Structural and corrosion behaviour of stoichiometric and substoichiometricTiN thin films. Surf Coat Technol 2004;180:158–63.
[20] Maury F, Duminica FD. TiO_xN_y coatings grown by atmospheric pressure metal organic chemical vapor deposition. Surf Coat Technol 2010;205:1287–93.
[21] Duminica FD, Maury F, Hausbrand R. N-doped TiO_2 coatings grown by atmospheric pressure MOCVD for visible light-induced photocatalytic activity. Surf Coat Technol 2007;201:9349–53.
[22] Farkas B, Heszler P, Budai J, et al. Optical, compositional and structural properties of pulsed laser deposited nitrogen-doped titanium-dioxide. Appl Surf Sci 2018;433:149–54.
[23] Madhavi V, Kondaiah P, Rao GM. Influence of silver nanoparticles on titanium oxide and nitrogen doped titanium oxide thin films for sun light photocatalysis. Appl Surf Sci 2018;436:708–19.
[24] Powell MJ, Dunnill CW, Parkin IP. N-doped TiO_2 visible light photocatalyst films via a sol–gel route using TMEDA as the nitrogen source. J PhotochemPhotobiol A: Chem 2014;281:27–34.
[25] Pierson HO. Handbook of chemical vapor deposition (CVD) – principles, technology and applications. 2ª ed. Noyes Publ.; 1999.
[26] Choy KL. Chemical vapour deposition of coatings. Prog Mater Sci 2008;48:57–170.
[27] Singh MP, Shivastrankar SA. Low pressure MOCVD of Al_2O_3 films using aluminum acetilacetonate as precursor: nucleation and growth. Surf Coat Technol 2002;161:135–43.
[28] Bonnet G, Aguilar G, Colson JC, et al. The effect of rare earths deposited on steel surfaces by different processes (sol/gel, electrophoresis, OMCVD) on high temperature corrosion behaviour. Corros Sci 1993;35:893–9.
[29] Quéré D. Wetting and roughness. Annu Rev Mater Res 2008;38:71–99.
[30] Yuan Y, Lee TR. Contact angle and wetting properties. Surf. Sci Technol 2013:3–34.
[31] Su M-J, Bai S, Luo Y, Chu G-W, Sun B-C, Le Y. Controllable wettability on stainless steel substrates with highly stable coatings. Chem Eng Sci 2019;195:791–800.
[32] Gao XF, Jiang L. Water-repellent legs of water striders. Nature 2004;432:63.
[33] Parker AR, Lawrence CR. Water capture by a desert beetle. Nature 2001;414:33–4.
[34] Krumdieck S, Gorthy R, Gardecka AJ, et al. Characterization of photocatalytic, wetting and optical properties of TiO_2 thin films and demonstration of uniform coating on a 3-D surface in the mass transport controlled regime. Surf Coat Technol 2017;326:402–10.
[35] Acik IO, Kiisk V, Krunks M, et al. Characterization of samarium and nitrogen co-doped TiO_2 films prepared by chemical spray pyrolysis. Appl Surf Sci 2012;261:735–41.
[36] Rojviroon T, Laobuthee A, Sirivithayapakorn S. Photocatalytic activity of toluene under UV-LED light with TiO_2 thin films. Int. J. Photoen 2012, http://dx.doi.org/10.1155/2012/898464 [8p.].
[37] Babelon P, Dequiedt AS, Mostefa-Sba H, et al. SEM and XPS studies of titanium dioxide thin films grown by MOCVD. Thin Solid Films 1998;322:63–7.
[38] Liu R, Zhou X, Yang F, et al. Combination study of DFT calculation and experiment for photocatalytic properties of S-doped anatase TiO_2. Appl Surf Sci 2014;319:50–9.
[39] Du J, Zhao G, Shi Y, et al. A facile method for synthesis of N-doped TiO_2nanooctahedra, nanoparticles, and nanospheres and enhanced photocatalytic activity. Appl Surf Sci 2013;273:278–86.

[40] Yang G, Jiang Z, Shi H, et al. Preparation of highly visible-light active N-doped TiO_2 photocatalyst. J Mater Chem 2010;20:5301–9.
[41] Peng F, Cai L, Yu H, et al. Synthesis and characterization of substitutional and interstitial nitrogen-doped titanium dioxides with visible light photocatalytic activity. J Sol State Chem 2008;181:130–6.
[42] Yates HM, Nolan MG, Shell DW, et al. The role of nitrogen doping on the development of visible light-induced photocatalytic activity in thin TiO_2 films grown on glass by chemical vapour deposition. J PhotochemPhotobiol A: Chem 2006;179:213–23.
[43] Shum PW, Zhou ZF, Li KY, et al. XPS, AFM and Nanoindentation studies of $Ti_{1-x}Al_xN$ films synthesized by reactive unbalanced magnetron sputtering. Mater Sci Eng B 2003;100:204–13.
[44] Chen X, Burda C. Photoelectron spectroscopic investigation of nitrogen-doped titania nanoparticles. J Phys Chem B 2004;108:15446–9.
[45] Mahidashti Z, Ramezanzadeh B. Influence of lanthanum as additive and post-treatment on the corrosion protection properties and surface morphology of mild steel chemically treated by a cerium conversion coating. J. Rare Earth 2018;36:1112–20.
[46] Maid MT, Shahrabi T, Ramezanzadeh B. Production of an eco-friendly anti-corrosion ceramic base nanostructured hybrid-film based on Nd (III)-$C_7H_6N_2$ on the mild steel surface; Electrochemical and surface studies. Constr Build Mater 2019;221:456–68.
[47] Maid MT, Shahrabi T, Ramezanzadeh B. The role of neodymium based thin film on the epoxy/steel interfacial adhesion and corrosion protection promotion. Appl Surf Sci 2019;464:516–33.
[48] Padhy N, Kamal S, Chandra R, et al. Corrosion performance of TiO_2 coated type 304L stainless steel in nitric acid medium. Surf Coat Technol 2010;204:2782–8.
[50] Wang H, Zhang R, Yuan Z, et al. A comparative study of titanium (Ti), titanium nitride (TiN), titanium dioxide (TiO_2) and nitrogen-doped titanium oxides (N-TiO_2), as coatings for biomedical applications. Ceram Int 2015;41:11844–51.
[51] Drelich J, Chibowski E, Meng DD, Terpilowski K. Hydrophilic and superhydrophilic surfaces and materials. Soft Matter 2011;7:9804–28.
[52] Ullah H, Kiran R. Influence of corrosion and surface roughness on wettability of ASTM A36 steels. J. Construct Steel Res 2018;144:310–26.